

A Multiparametric Class of Low-complexity Transforms for Image and Video Coding

Diego Ramos Canterle* Thiago L. T. da Silveira[†] Fábio Mariano Bayer[‡] Renato J. Cintra[§]

Abstract

Discrete transforms play an important role in many signal processing applications, and low-complexity alternatives for classical transforms became popular in recent years. Particularly, the discrete cosine transform (DCT) has proven to be convenient for data compression, being employed in well-known image and video coding standards such as JPEG, H.264, and the recent high efficiency video coding (HEVC). In this paper, we introduce a new class of low-complexity 8-point DCT approximations based on a series of works published by Bouguezel, Ahmed and Swamy. Also, a multiparametric fast algorithm that encompasses both known and novel transforms is derived. We select the best-performing DCT approximations after solving a multicriteria optimization problem, and submit them to a scaling method for obtaining larger size transforms. We assess these DCT approximations in both JPEG-like image compression and video coding experiments. We show that the optimal DCT approximations present compelling results in terms of coding efficiency and image quality metrics, and require only few addition or bit-shifting operations, being suitable for low-complexity and low-power systems.

Keywords

Approximate transforms, Arithmetic complexity, Discrete cosine transform, Image compression, Video coding.

1 Introduction

The discrete cosine transform (DCT) [1] is a fundamental tool in the digital signal processing field [2,3]. More precisely, the DCT is an asymptotic data-independent approximation for the optimal Karhunen-Love transform (KLT) [4] when the input signal can be modeled as a first-order Markovian process, and the signal correlation coefficient tends to the unit ($\rho \rightarrow 1$) [5]. Natural images are signals that belong to this statistical class [6].

The DCT has been successfully employed in well-known image and video coding standards, like JPEG [7], H.264 [8] and the recent high efficiency video coding (HEVC) [9]. Several DCT methods, such as [10–13], led to block-based transformations equipped with fast algorithms that are capable of acceptable computational burden and are widely adopted for efficient encoding of both images and video sequences.

Nevertheless, due to the irrational quantities in the DCT formulation, exact transformations might entail realizations that require relatively demanding arithmetic schemes [14], such as floating-point or large integer fixed-point systems. Such constraint can preclude the applicability of the exact DCT computation in extremely low-power and real-time systems [15–17], such as [18,19]. In this context, approximate transforms can be efficiently implemented using only addition and bit-shifting operations [17,20–24]. In fact, there are several methods in literature that focus on finding a good compromise between coding efficiency and computational cost [17,21–42]. Classically, special attention was given to 8-point approximate transforms, since this particular blocklength is employed in both JPEG and H.264 coding standards. Nowadays, transforms of larger sizes, such as $N = 16, 32$ are also required to cope with high-resolution video coding [9,35,43].

*D. R. Canterle is with the Instituto de Matemática e Estatística, Universidade de São Paulo, São Paulo, Brazil; and was with the Programa de Pós-Graduação em Engenharia Elétrica, Universidade Federal de Pernambuco, Recife, Brazil, e-mail: diegocanterle@gmail.com

[†]T. L. T. da Silveira is with the Centro de Ciências Computacionais, Universidade Federal do Rio Grande, Rio Grande, Brazil, e-mail: tltsilveira@furg.br

[‡]F. M. Bayer is with the Departamento de Estatística and LACESM, Universidade Federal de Santa Maria, Santa Maria, RS, Brazil, e-mail: bayer@ufsm.br

[§]R. J. Cintra is with the Signal Processing Group, Departamento de Estatística, Universidade Federal de Pernambuco, Recife, Brazil; and the Department of Electrical and Computer Engineering, University of Calgary, Calgary, AB, Canada., e-mail: rjdc@de.ufpe.br

A number of works proposing 8-point multiplication-free transforms in the context of image compression was introduced by Bouguezel-Ahmad-Swamy (BAS) [17, 24, 31–34]. In particular, we emphasize the method described in [24] which employs a single parameter approximation for the 8-point DCT. We aim at significantly extending such parameter-based approach.

In this paper, we propose a new multiparametric class of low-complexity 8-point DCT approximations that encompasses the BAS transforms, and present the underlying fast algorithm. The obtained DCT approximations in the proposed class of low-complexity transforms are sought to be assessed and screened through an optimization process considering proximity measures relative to the exact DCT and coding efficiency metrics. Then, the best-performing transforms are submitted to a scaling method for obtaining 16- and 32-point DCT approximations, aiming at the application in recent image and video encoders [9, 44].

The rest of the paper is organized as follows. Section 2 presents the mathematical formulation of the new class of DCT approximations. In Section 3, we explain the proposed multicriteria optimization scheme, and show the resulting 8-point low-complexity transforms. Section 4 introduces novel 16- and 32-point DCT approximations generated by the scaling method from [45]. Sections 5 and 6 present, respectively, image and video coding experiments. Finally, Section 7 concludes this work.

2 Multiparametric DCT approximations

In this section, we review the DCT and introduce the mathematical formulation for the proposed class of low-complexity transforms. Computational complexity and orthogonality property are derived and discussed.

2.1 A review about the DCT

Let \mathbf{C}_N be the transformation matrix related to the N -point DCT, for which the elements are given by [1]

$$c_{i,j} = \alpha_i \cos\left(\frac{\pi i(2j+1)}{2N}\right),$$

where $i, j = 0, 1, \dots, N-1$, and

$$\alpha_k = \begin{cases} 1/\sqrt{N}, & \text{if } k = 0, \\ \sqrt{2/N}, & \text{if } k > 0. \end{cases}$$

Considering the standard approach for splitting images into disjoint sub-blocks [46], the blockwise forward and inverse two-dimensional DCT transformation are given, respectively, by [1]

$$\mathbf{B} = \mathbf{C}_N \cdot \mathbf{A} \cdot \mathbf{C}_N^\top \tag{1}$$

and

$$\mathbf{A} = \mathbf{C}_N^\top \cdot \mathbf{B} \cdot \mathbf{C}_N, \tag{2}$$

where \mathbf{A} and \mathbf{B} represent the input and transformed $N \times N$ signals, respectively. Note that because \mathbf{C}_N is orthogonal, the inverse transformation is immediately obtained by matrix transposition. In practical terms, orthogonality implies that the both forward and inverse transformations share similar realizations [2].

Hereafter, we use the notation $\hat{\mathbf{C}}$ for referring to a given *DCT approximation*. Generally, DCT approximations can be written as $\hat{\mathbf{C}} = \mathbf{S} \cdot \mathbf{T}$, where \mathbf{S} is a diagonal scaling matrix and \mathbf{T} is a low-complexity matrix whose entries are in the set $\mathcal{C} = \{0, \pm 0.5, \pm 1, \pm 2\}$. Details are given in Section 2.5.

2.2 Parametrization

Most BAS low-complexity transforms can be understood as variations of the signed DCT (SDCT) [20] according to judicious changes in the matrix entries. The SDCT can be obtained for any transform size N by applying the signum function to all the entries of \mathbf{C}_N . The resulting transformation matrix contains only elements in the set $\{\pm 1\}$ and can be implemented using only additions, i.e., multiplications or bit-shifting operations are not required. However, as a drawback, the SDCT lacks orthogonality for $N \neq 4$.

Based on the 8-point BAS orthogonal transforms reported in the literature [17, 24, 31, 33, 34], we aim at proposing a parametrization capable of encompassing such DCT approximations. To attain the sought multiparametric class of BAS-based transforms, we perform entry-wise comparisons of the considered BAS transforms keeping common matrix blocks and parametrizing the variations. Thus the proposed multiparametric class of DCT approximations based on BAS transforms is given by the following expression:

$$\mathbf{T}(\mathbf{a}) = \begin{bmatrix} 1 & 1 & 1 & 1 & 1 & 1 & 1 & 1 \\ 1 & 1 & a_1 & a_1 & -a_1 & -a_1 & -1 & -1 \\ 1 & a_2 & -a_2 & -1 & -1 & -a_2 & a_2 & 1 \\ a_1 & a_3 & -a_4 & -a_1 & a_1 & a_4 & -a_3 & -a_1 \\ 1 & -1 & -1 & 1 & 1 & -1 & -1 & 1 \\ a_5 & -a_5 & -a_1 & a_6 & -a_6 & a_1 & a_5 & -a_5 \\ a_2 & -1 & 1 & -a_2 & -a_2 & 1 & -1 & a_2 \\ a_7 & -a_6 & a_1 & -a_8 & a_8 & -a_1 & a_6 & -a_7 \end{bmatrix}, \quad (3)$$

where $\mathbf{a} = [a_1 \ a_2 \ a_3 \ a_4 \ a_5 \ a_6 \ a_7 \ a_8]^\top \in \mathbb{R}^8$ is the parameter vector for matrix generation. Depending on the values of \mathbf{a} we can find different transforms as special cases, such as those proposed in [17, 24, 31, 33, 34]. In order to guarantee low-complexity transforms we shall consider that $a_i \in \mathcal{C}$, for $i = 1, \dots, 8$.

Note that reducing the computational complexity is only one possible requirement. Since we are interested in exploring BAS-based transforms in the context of image and video coding, it is also important to attain good compaction properties [14]. BAS transforms do have high coding gain and transform efficiency measurements [31, 33, 34, 42], and we expect to find novel transforms sharing the same properties (cf. Section 3).

2.3 Fast algorithm

Following similar approach as in [21–23, 35], we sparsely factorize the low-complexity matrix given in Equation (3) as

$$\mathbf{T}(\mathbf{a}) = \mathbf{P} \cdot \mathbf{K}(\mathbf{a}) \cdot \mathbf{A}_2 \cdot \mathbf{A}_1,$$

where

$$\mathbf{A}_1 = \begin{bmatrix} 1 & 0 & 0 & 0 & 0 & 0 & 0 & 1 \\ 0 & 1 & 0 & 0 & 0 & 0 & 1 & 0 \\ 0 & 0 & 1 & 0 & 0 & 1 & 0 & 0 \\ 0 & 0 & 0 & 1 & 1 & 0 & 0 & 0 \\ 0 & 0 & 0 & 1 & -1 & 0 & 0 & 0 \\ 0 & 0 & 1 & 0 & 0 & -1 & 0 & 0 \\ 0 & 1 & 0 & 0 & 0 & 0 & -1 & 0 \\ 1 & 0 & 0 & 0 & 0 & 0 & 0 & -1 \end{bmatrix},$$

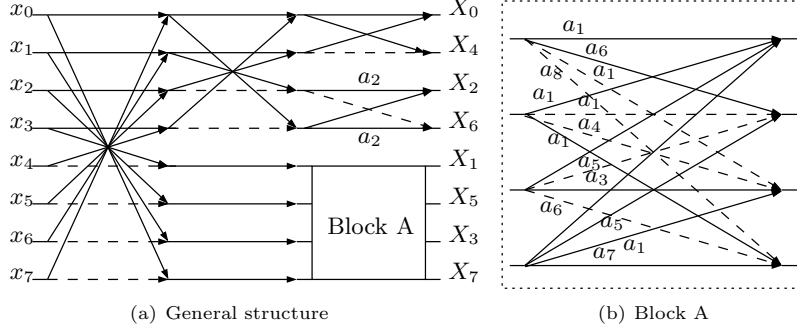


Figure 1: SFG for $\mathbf{T}(\mathbf{a})$. Input data $x_i, i = 0, 1, \dots, 7$, relates to output $X_j, j = 0, 1, \dots, 7$, according to $X = \mathbf{T}(\mathbf{a}) \cdot x$. Dashed arrows represent multiplications by -1 .

$$\mathbf{A}_2 = \begin{bmatrix} 1 & 0 & 0 & 1 & 0 & 0 & 0 & 0 \\ 0 & 1 & 1 & 0 & 0 & 0 & 0 & 0 \\ 0 & 1 & -1 & 0 & 0 & 0 & 0 & 0 \\ 1 & 0 & 0 & -1 & 0 & 0 & 0 & 0 \\ 0 & 0 & 0 & 0 & 1 & 0 & 0 & 0 \\ 0 & 0 & 0 & 0 & 0 & 1 & 0 & 0 \\ 0 & 0 & 0 & 0 & 0 & 0 & 1 & 0 \\ 0 & 0 & 0 & 0 & 0 & 0 & 0 & 1 \end{bmatrix},$$

$$\mathbf{K}(\mathbf{a}) = \begin{bmatrix} 1 & 1 & 0 & 0 & 0 & 0 & 0 & 0 \\ 1 & -1 & 0 & 0 & 0 & 0 & 0 & 0 \\ 0 & 0 & a_2 & 1 & 0 & 0 & 0 & 0 \\ 0 & 0 & -1 & a_2 & 0 & 0 & 0 & 0 \\ 0 & 0 & 0 & 0 & a_1 & a_1 & 1 & 1 \\ 0 & 0 & 0 & 0 & a_6 & -a_1 & -a_5 & a_5 \\ 0 & 0 & 0 & 0 & -a_1 & -a_4 & a_3 & a_1 \\ 0 & 0 & 0 & 0 & -a_8 & a_1 & -a_6 & a_7 \end{bmatrix},$$

and

$$\mathbf{P} = \begin{bmatrix} 1 & 0 & 0 & 0 & 0 & 0 & 0 & 0 \\ 0 & 0 & 0 & 0 & 1 & 0 & 0 & 0 \\ 0 & 0 & 1 & 0 & 0 & 0 & 0 & 0 \\ 0 & 0 & 0 & 0 & 0 & 0 & 1 & 0 \\ 0 & 1 & 0 & 0 & 0 & 0 & 0 & 0 \\ 0 & 0 & 0 & 0 & 0 & 1 & 0 & 0 \\ 0 & 0 & 0 & 1 & 0 & 0 & 0 & 0 \\ 0 & 0 & 0 & 0 & 0 & 0 & 0 & 1 \end{bmatrix}.$$

Note that only matrix $\mathbf{K}(\mathbf{a})$ depends on the parameter vector \mathbf{a} . The signal flow graph (SFG) for the proposed fast algorithm is shown in Figure 1. We discuss in detail the computational complexity associated to $\mathbf{T}(\mathbf{a})$ in the following.

2.4 Computational complexity

Matrices \mathbf{A}_1 and \mathbf{A}_2 contribute with additions only. Matrix \mathbf{P} represents a permutation, which is multiplierless and corresponds to wiring in terms of circuit implementation. The computational complexity of matrix $\mathbf{K}(\mathbf{a})$ depends on the parameter vector \mathbf{a} . Here, we consider that the elements of \mathbf{a} are in the set \mathcal{C} , so that only additions and bit-shifting operations are required for implementing the fast algorithms of $\mathbf{T}(\mathbf{a})$ (see Figure 1).

Thus, the number of additions $\mathcal{A}(\mathbf{a})$ and bit-shifting operations $\mathcal{S}(\mathbf{a})$ required for implementing $\mathbf{T}(\mathbf{a})$ are given, respectively, by

$$\mathcal{A}(\mathbf{a}) = 28 - \sum_{i=1}^8 w_i \mathcal{I}_{\{0\}}(a_i) \quad \text{and} \quad \mathcal{S}(\mathbf{a}) = \sum_{i=1}^8 w_i \mathcal{I}_{\{\frac{1}{2}, 2\}}(a_i),$$

where $\mathbf{w} = [62112211]^\top$, and $\mathcal{I}_X(x) = 1$, if $x \in X$, otherwise it returns zero.

These equations compute additive and bit-shift complexity considering the fast algorithm presented in Figure 1. This fast algorithm is general and the arithmetic complexity can be further reduced depending on the parameter vector \mathbf{a} . Specific combinations of the scalars within \mathbf{a} lead to simplified versions of \mathbf{A}_2 and $\mathbf{K}(\mathbf{a})$ that require fewer computations. We list all nine restrictions and their modified addition and bit-shifting counts below.

1. If $|a_1| = |a_4| = |a_6| = |a_8|$, then

$$\mathcal{A}(\mathbf{a}) = 26 - \sum_{i=1}^8 w_i \mathcal{I}_{\{0\}}(a_i) \quad \text{and} \quad \mathcal{S}(\mathbf{a}) = \sum_{i=1}^8 w_i \mathcal{I}_{\{\frac{1}{2}, 2\}}(a_i),$$

where $\mathbf{w} = [62102010]^\top$;

2. If $(|a_1| = |a_3| = 1) \wedge (|a_5| = |a_6| = |a_8|)$, then

$$\mathcal{A}(\mathbf{a}) = 26 - \sum_{i=1}^8 w_i \mathcal{I}_{\{0\}}(a_i) \quad \text{and} \quad \mathcal{S}(\mathbf{a}) = \sum_{i=1}^8 w_i \mathcal{I}_{\{\frac{1}{2}, 2\}}(a_i),$$

where $\mathbf{w} = [02013010]^\top$;

3. If $(|a_1| = 1) \wedge (|a_5| = |a_6|) \wedge (|a_7| = |a_8|)$, then

$$\mathcal{A}(\mathbf{a}) = 26 - \sum_{i=1}^8 w_i \mathcal{I}_{\{0\}}(a_i) \quad \text{and} \quad \mathcal{S}(\mathbf{a}) = \sum_{i=1}^8 w_i \mathcal{I}_{\{\frac{1}{2}, 2\}}(a_i),$$

where $\mathbf{w} = [02113010]^\top$;

4. If $(|a_1| = |a_5| = |a_6| = 1) \wedge (|a_3| = |a_4|)$, then

$$\mathcal{A}(\mathbf{a}) = 26 - \sum_{i=1}^8 w_i \mathcal{I}_{\{0\}}(a_i) \quad \text{and} \quad \mathcal{S}(\mathbf{a}) = \sum_{i=1}^8 w_i \mathcal{I}_{\{\frac{1}{2}, 2\}}(a_i),$$

where $\mathbf{w} = [02100011]^\top$;

5. If $|a_1| = |a_4| = |a_5| = |a_7| = 1$, then

$$\mathcal{A}(\mathbf{a}) = 26 - \sum_{i=1}^8 w_i \mathcal{I}_{\{0\}}(a_i) \quad \text{and} \quad \mathcal{S}(\mathbf{a}) = \sum_{i=1}^8 w_i \mathcal{I}_{\{\frac{1}{2}, 2\}}(a_i),$$

where $\mathbf{w} = [02100201]^\top$;

6. If $(|a_1| = |a_3|) \wedge (|a_6| = |a_7|)$, then

$$\mathcal{A}(\mathbf{a}) = 26 - \sum_{i=1}^8 w_i \mathcal{I}_{\{0\}}(a_i) \quad \text{and} \quad \mathcal{S}(\mathbf{a}) = \sum_{i=1}^8 w_i \mathcal{I}_{\{\frac{1}{2}, 2\}}(a_i),$$

where $\mathbf{w} = [62011201]^\top$;

7. If $|a_1| = |a_3| = |a_4| = |a_6| = |a_7| = |a_8|$, then

$$\mathcal{A}(\mathbf{a}) = 24 - \sum_{i=1}^8 w_i \mathcal{I}_{\{0\}}(a_i) \quad \text{and} \quad \mathcal{S}(\mathbf{a}) = \sum_{i=1}^8 w_i \mathcal{I}_{\{\frac{1}{2}, 2\}}(a_i),$$

where $\mathbf{w} = [62001000]^\top$;

8. If $|a_1| = |a_3| = |a_4| = |a_5| = |a_6| = |a_7| = |a_8| = 1$, then

$$\mathcal{A}(\mathbf{a}) = 24 - \sum_{i=1}^8 w_i \mathcal{I}_{\{0\}}(a_i) \quad \text{and} \quad \mathcal{S}(\mathbf{a}) = \sum_{i=1}^8 w_i \mathcal{I}_{\{\frac{1}{2}, 2\}}(a_i),$$

where $\mathbf{w} = [02000000]^\top$;

9. If $(|a_1| = |a_5| = |a_6| = 1) \wedge (|a_3| = |a_4|) \wedge (|a_7| = |a_8|)$, then

$$\mathcal{A}(\mathbf{a}) = 24 - \sum_{i=1}^8 w_i \mathcal{I}_{\{0\}}(a_i) \quad \text{and} \quad \mathcal{S}(\mathbf{a}) = \sum_{i=1}^8 w_i \mathcal{I}_{\{\frac{1}{2}, 2\}}(a_i),$$

where $\mathbf{w} = [02100010]^\top$.

Above expressions show that $16 \leq \mathcal{A}(\mathbf{a}) \leq 28$ and $0 \leq \mathcal{S}(\mathbf{a}) \leq 16$.

2.5 Orthogonality and orthonormality

Discrete transforms are often required to be orthogonal [14, 47]. One of the reasons is the fact that orthogonality ensures that the good mathematical properties of the forward transformation are transferred to the inverse operation.

Here, a matrix \mathbf{T} is said to be orthogonal if $\mathbf{T} \cdot \mathbf{T}^\top$ is a diagonal matrix. If $\mathbf{T} \cdot \mathbf{T}^\top$ is the identity matrix then \mathbf{T} is referred to as orthonormal. Considering the proposed parametrization (Equation (3)), we have:

$$\mathbf{T}(\mathbf{a}) \cdot \mathbf{T}(\mathbf{a})^\top = \begin{bmatrix} 8 & 0 & 0 & 0 & 0 & 0 & 0 & 0 \\ 0 & \tau_1 & 0 & \tau_6 & 0 & \tau_7 & 0 & \tau_8 \\ 0 & 0 & \tau_2 & 0 & 0 & 0 & 0 & 0 \\ 0 & \tau_6 & 0 & \tau_3 & 0 & \tau_9 & 0 & \tau_{10} \\ 0 & 0 & 0 & 0 & 8 & 0 & 0 & 0 \\ 0 & \tau_7 & 0 & \tau_9 & 0 & \tau_4 & 0 & \tau_{11} \\ 0 & 0 & 0 & 0 & 0 & 0 & \tau_2 & 0 \\ 0 & \tau_8 & 0 & \tau_{10} & 0 & \tau_{11} & 0 & \tau_5 \end{bmatrix},$$

where $\tau_1 = 4a_1^2 + 4$, $\tau_2 = 4a_2^2 + 4$, $\tau_3 = 4a_1^2 + 2a_3^2 + 2a_4^2$, $\tau_4 = 2a_6^2 + 4a_5^2 + 2a_1^2$, $\tau_5 = 2a_8^2 + 2a_7^2 + 2a_6^2 + 2a_1^2$, $\tau_6 = 2a_1 - 2a_1^2 + 2a_3 - 2a_1a_4$, $\tau_7 = 2a_1a_6 - 2a_1^2$, $\tau_8 = 2a_1^2 - 2a_6 + 2a_7 - 2a_1a_8$, $\tau_9 = 2a_1a_4 + 2a_1a_5 - 2a_3a_5 - 2a_1a_6$, $\tau_{10} = 2a_1a_8 + 2a_1a_7 - 2a_3a_6 - 2a_1a_4$ and $\tau_{11} = 2a_5a_7 + 2a_5a_6 - 2a_1^2 - 2a_6a_8$. Matrix $\mathbf{T}(\mathbf{a})$ is orthogonal, if its entries τ_6 , τ_7 , τ_8 , τ_9 , τ_{10} , and τ_{11} are equal to zero. Therefore, the following conditions must hold true to ensure orthogonality:

$$\begin{cases} 2a_1 - 2a_1^2 + 2a_3 - 2a_1a_4 & = 0, \\ 2a_1a_6 - 2a_1^2 & = 0, \\ 2a_1^2 - 2a_6 + 2a_7 - 2a_1a_8 & = 0, \\ 2a_1a_4 + 2a_1a_5 - 2a_3a_5 - 2a_1a_6 & = 0, \\ 2a_1a_8 + 2a_1a_7 - 2a_3a_6 - 2a_1a_4 & = 0, \\ 2a_5a_7 + 2a_5a_6 - 2a_1^2 - 2a_6a_8 & = 0. \end{cases}$$

Orthonormality can be obtained by means of polar decomposition [21, 22, 25]. An orthonormal DCT approximation

$\hat{\mathbf{C}}(\mathbf{a})$ is given by [48]

$$\hat{\mathbf{C}}(\mathbf{a}) = \mathbf{S}(\mathbf{a}) \cdot \mathbf{T}(\mathbf{a}),$$

where

$$\mathbf{S}(\mathbf{a}) = \sqrt{\left[\mathbf{T}(\mathbf{a}) \cdot \mathbf{T}(\mathbf{a})^\top\right]^{-1}},$$

and $\sqrt{\cdot}$ denotes the matrix square root [49]. Thus, we have that

$$\mathbf{S}(\mathbf{a}) = \text{diag}\left(\frac{1}{2\sqrt{2}}, \frac{1}{\sqrt{71}}, \frac{1}{\sqrt{72}}, \frac{1}{\sqrt{73}}, \frac{1}{2\sqrt{2}}, \frac{1}{\sqrt{74}}, \frac{1}{\sqrt{72}}, \frac{1}{\sqrt{75}}\right).$$

However, in the context of image and video coding, not only $\mathbf{T}(\mathbf{a})$ is said to be of low-complexity but also $\hat{\mathbf{C}}(\mathbf{a})$ because the scaling matrix $\mathbf{S}(\mathbf{a})$ can be merged in the quantization step [21, 22, 24, 28, 31, 33, 47]. Therefore, $\mathbf{S}(\mathbf{a})$ does not contribute with any computational complexity.

3 Multicriteria optimization

In this section, we employ multicriteria optimization for finding DCT approximations according to the mathematical formalism discussed in the previous section. Frequently, two types of metrics are used for assessing a given approximate DCT [23]: proximity measures and coding measures. Proximity measures assess how close this transform is to the exact DCT in a Euclidean sense, implying the low measurements are sought. On the other hand, coding measures aim at capturing how good a transformation is in terms of energy compaction properties; high values of coding are desirable. Total error energy [22] and mean square error (MSE) [14] are adopted as proximity measures; whereas coding gain [50] and transform efficiency [14] are selected for coding measurements. Moreover, the number of additions and number of bit-shift operations are also considered as figures of metric for complexity and are sought to be minimized. The above discussion entails the following multicriteria minimization problem:

$$\min_{\mathbf{a}}(\epsilon(\hat{\mathbf{C}}(\mathbf{a})), \text{MSE}(\hat{\mathbf{C}}(\mathbf{a})), -C_g^*(\hat{\mathbf{C}}(\mathbf{a})), -\eta(\hat{\mathbf{C}}(\mathbf{a})), \mathcal{A}(\mathbf{a}), \mathcal{S}(\mathbf{a})), \quad (4)$$

where $\epsilon(\cdot)$, $\text{MSE}(\cdot)$, $C_g^*(\cdot)$, and $\eta(\cdot)$ compute, respectively, the total error energy, the mean square error, the unified coding gain and the transform efficiency. When necessary, $\mathcal{A}(\mathbf{a})$ and $\mathcal{S}(\mathbf{a})$ are computed according to the restrictions on the elements of \mathbf{a} described in Section 2.4.

For $a_i \in \mathcal{C}$, $i = 1, 2, \dots, 8$, then there are $7^8 = 5,764,801$ candidate matrices in the search space of (4). Thus, the above problem can be solved by means of exhaustive search in contemporary computers. The exhaustive search demanded four weeks of uninterrupted calculations in a computer with an Intel Core i5 (3th generation) processor equipped with 6GB of RAM running R language [51] on Linux OS (Ubuntu 16.04 LTS).

Table 1 presents the obtained fifteen optimal solutions of (4). For the sake of simplicity, we refer to the optimal 8-point DCT approximations as $\hat{\mathbf{C}}_{8,j}$, $j = 1, 2, \dots, 15$. Note that $\hat{\mathbf{C}}_{8,2}$, $\hat{\mathbf{C}}_{8,5}$, and $\hat{\mathbf{C}}_{8,15}$ coincide with literature results [31, 33, 34]. The transform $\hat{\mathbf{C}}_{8,1}$ was previously published in [42, 52], which consists of judiciously changing few entries of the matrix describes in [53] leading to orthogonalization. To the best of our knowledge, the remaining eleven matrices are novel results.

Table 2 displays the proximity and coding measurements, as well as arithmetic complexity, for the obtained approximations. The best measurements are highlighted in boldface. The approximation $\hat{\mathbf{C}}_{8,15}$ attained the best results for proximity and coding metrics. However, as a trade-off, $\hat{\mathbf{C}}_{8,15}$ has the highest computational complexity. The approximation with the lowest computational cost is $\hat{\mathbf{C}}_{8,1}$. Among the new transforms, $\hat{\mathbf{C}}_{8,9}$ is worth-mentioning for its proximity to the exact DCT, and $\hat{\mathbf{C}}_{8,14}$ and $\hat{\mathbf{C}}_{8,12}$, for the high coding gain and transform efficiency, respectively.

For further comparison, we show the performance measurements of the following competing DCT approximations

Table 1: Optimal 8-point DCT approximations

j	\mathbf{a}	Comment
1	$[00011001]^\top$	[42, 52]
2	$[01011001]^\top$	[33]
3	$[00010.5111]^\top$	New transform
4	$[00011112]^\top$	New transform
5	$[00.5011001]^\top$	[31]
6	$[10001100]^\top$	New transform
7	$[01011112]^\top$	New transform
8	$[01010.5111]^\top$	New transform
9	$[00.5011112]^\top$	New transform
10	$[00.5010.5111]^\top$	New transform
11	$[10111111]^\top$	New transform
12	$[10.5001100]^\top$	New transform
13	$[100.50.5110.50.5]^\top$	New transform
14	$[10.5111111]^\top$	New transform
15	$[10.50.50.5110.50.5]^\top$	[34]

Table 2: Results for the optimal 8-point DCT approximations.

j	$\epsilon(\cdot)$	MSE(\cdot)	$C_g^*(\cdot)$	$\eta(\cdot)$	$\mathcal{A}(\cdot)$	$\mathcal{S}(\cdot)$
1	6.85	0.03	7.91	85.64	16	0
2	6.85	0.03	7.91	85.38	18	0
3	5.79	0.03	7.91	85.78	18	1
4	5.05	0.03	7.91	85.51	18	1
5	5.93	0.02	8.12	86.86	18	2
6	6.85	0.03	7.93	85.80	20	0
7	5.05	0.03	7.91	85.25	20	1
8	5.79	0.03	7.91	85.52	20	1
9	4.12	0.02	8.12	86.73	20	3
10	4.87	0.02	8.12	87.01	20	3
11	5.05	0.02	7.95	85.58	22	0
12	5.93	0.02	8.14	87.02	22	2
13	5.02	0.02	8.12	86.96	22	2
14	4.12	0.02	8.15	86.79	24	2
15	4.09	0.02	8.33	88.22	24	4

Table 3: Results for competing 8-point DCT approximations.

Transform	$\epsilon(\cdot)$	MSE(\cdot)	$C_g^*(\cdot)$	$\eta(\cdot)$	$\mathcal{A}(\cdot)$	$\mathcal{S}(\cdot)$
BAS ₅ (0) [24]	26.86	0.07	7.91	85.64	16	0
FW ₆ [23]	3.32	0.02	6.05	83.08	18	0
BAS ₃ [33]	6.85	0.03	7.91	85.38	18	0
BAS ₅ (1) [24]	26.86	0.07	7.91	85.38	18	0
BAS ₅ (1/2) [24]	26.40	0.07	8.12	86.86	18	2
BAS ₁ [31]	5.93	0.02	8.12	86.86	18	2
FW ₅ [23]	7.41	0.05	7.58	83.08	20	10
RDCT [22]	1.79	0.01	8.18	87.43	22	0
BAS ₆ [17]	35.06	0.10	7.95	85.31	24	0
LO [47]	0.87	0.01	8.39	88.70	24	2
BAS ₄ [34]	4.09	0.02	8.33	88.22	24	4
ABM [35]	1.22	0.01	8.63	90.46	24	6

that are out of our class of transformations defined in (3): FW₅ and FW₆ approximations from [23], the rounded discrete cosine transform (RDCT) [22], Lengwehasatit and Ortega level 1 approximation (LO) [47], and angle-based DCT approximation (ABM) [35]. We also list BAS transformations [17,24,31,33,34] that were not considered optimal according to our methodology but they are special cases of our class of transformations. The BAS transform proposed in [24] BAS₅(a) is a uniparametric transform, where a is the parameter. Table 3 summarizes the measurements.

Figure 2 relates the computational complexity to the four metrics in Equation (4) for all considered DCT approximations. The dotted curves refer to the Pareto boundary which indicates the optimal transforms for each case [54]. Considering transforms with 16 additions, $\hat{\mathbf{C}}_{8,1}$ [52] achieves the best measurements in terms of MSE and total error energy. Approximation $\hat{\mathbf{C}}_{8,1}$ presents identical results as the ones from the approximation BAS₅(0) when coding gain and transform efficiency are considered. Approximations FW₆ and BAS₁ attain the best results in terms of proximity to the exact DCT and coding efficiency, respectively, if a maximum of 18 additions is considered. When considering transforms that require 20 additions, $\hat{\mathbf{C}}_{8,9}$ performs better in terms of MSE, total energy error and coding gain. The highest transform efficiency is achieved by $\hat{\mathbf{C}}_{8,10}$. RDCT is the best-performing if compared to other transforms requiring 22 additions. Finally, for the case of 24 additions, LO transform achieves the minimum MSE, and ABM has the best results for the other metrics. Note that the transforms of our class of transformations requiring 16, 18, and 20 additions are usually the best-performing in terms of coding gain and transform efficiency.

4 Scaled optimal transforms

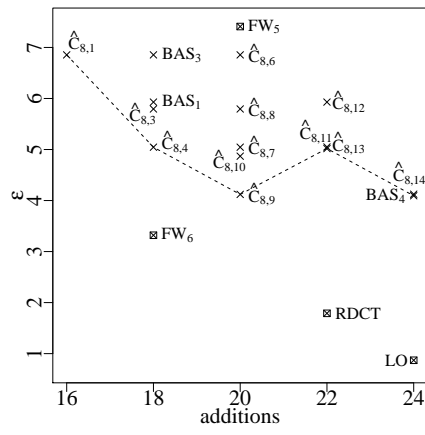
The widely popular HEVC standard adopts larger size transforms to produce high-resolution video coding [9]. In response, 16- and 32-point DCT approximations have been proposed [17,34,35,45,55,56]. In this work, we rely on the scaling method proposed by Jridi-Alfalou-Meher (JAM) [45] which takes as input a low-complexity transform of size N and generates a transform of size $2N$. We refer the reader to [45] for more details about the scaling procedure.

4.1 Proposed 16-point DCT approximations

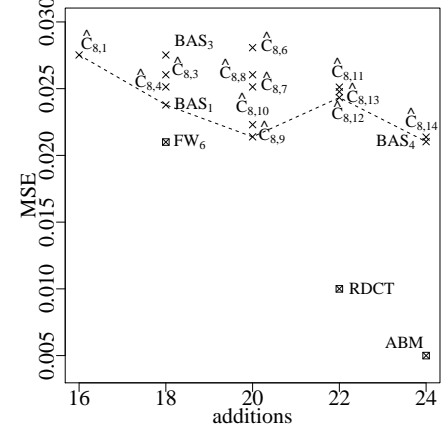
Following the JAM method, we obtain 16-point DCT approximations based on the parametrization shown in Equation (3), resulting in:

$$\mathbf{T}_{16}(\mathbf{a}) = \begin{bmatrix} \mathbf{T}_8(\mathbf{a}) & \mathbf{0}_8 \\ \mathbf{0}_8 & \mathbf{T}_8(\mathbf{a}) \end{bmatrix} \cdot \begin{bmatrix} \mathbf{I}_8 & \bar{\mathbf{I}}_8 \\ \mathbf{I}_8 & -\bar{\mathbf{I}}_8 \end{bmatrix}$$

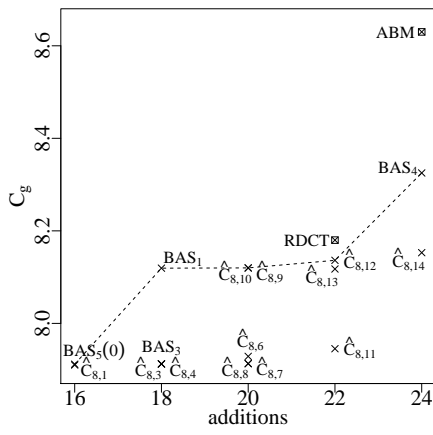
where $\mathbf{0}_8$ is 8×8 a matrix of zeros; \mathbf{I}_8 and $\bar{\mathbf{I}}_8$ are the identity and counter-identity matrices of order 8.



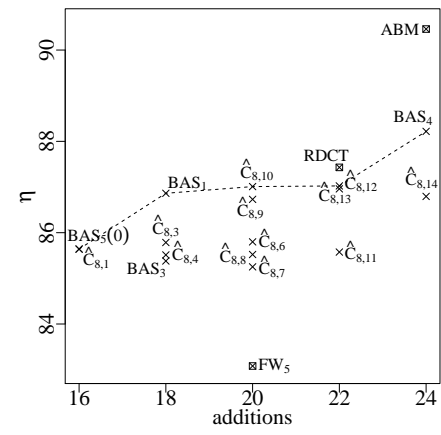
(a) Total energy error



(b) MSE



(c) Unified coding gain



(d) Transform efficiency

Figure 2: Assessment plots for the proposed efficient approximations and competing methods. Dashed line represents the Pareto boundary for the transforms belonging to the proposed class.

Table 4: Results for the novel 16-point DCT approximations.

j	$\epsilon(\cdot)$	MSE(\cdot)	$C_g^*(\cdot)$	$\eta(\cdot)$	$\mathcal{A}(\cdot)$	$\mathcal{S}(\cdot)$
1	25.13	0.07	8.16	70.98	48	0
2	24.27	0.07	8.16	70.80	52	0
3	21.75	0.07	8.16	71.25	52	2
4	20.88	0.06	8.16	71.48	52	2
5	23.02	0.06	8.37	71.83	52	4
6	22.46	0.06	8.18	71.29	56	0
7	20.02	0.06	8.16	71.30	56	2
8	20.89	0.06	8.16	71.06	56	2
9	18.77	0.06	8.37	72.34	56	6
10	19.64	0.06	8.37	72.10	56	6
11	18.29	0.06	8.19	70.83	60	0
12	20.35	0.06	8.38	72.14	60	4
13	18.52	0.06	8.36	72.63	60	4
14	16.18	0.06	8.40	71.67	64	4
15	16.41	0.06	8.57	73.51	64	8

Table 5: Results for competing 16-point DCT approximations.

Transform	$\epsilon(\cdot)$	MSE(\cdot)	$C_g^*(\cdot)$	$\eta(\cdot)$	$\mathcal{A}(\cdot)$	$\mathcal{S}(\cdot)$
SOBCM [56]	41.00	0.09	7.86	67.61	44	0
SBCKMK [55]	30.32	0.06	8.29	70.83	60	0
JAM ₁₆ [45]	14.74	0.05	8.43	72.23	60	0
BAS ₁₆ -2013 [17]	54.62	0.13	8.19	70.64	64	0
BAS ₁₆ -2010 [34]	16.41	0.06	8.52	73.63	64	8
ABM ₁₆ [35]	13.70	0.05	8.88	76.81	64	12
BCEM [28]	8.08	0.05	7.84	65.28	72	0

If the elements of \mathbf{a} are in the set \mathcal{C} , then $\mathbf{T}_{16}(\mathbf{a})$ is a low-complexity matrix. The computational cost of the resulting $2N$ -point transform is given by twice the number of bit-shifting operations of the original N -point transform; and twice the number of additions plus $2N$ extra additions.

Submitting the optimal 8-point DCT approximations from Table 2 to the JAM method results in fifteen novel 16-point transforms, which are shown in Table 4. We denote these 16-point DCT approximations as $\hat{\mathbf{C}}_{16,j}$, $j = 1, 2, \dots, 15$. Table 5 lists competing 16-point DCT approximations [17, 28, 34, 35, 45, 55, 56] for comparison purposes.

The approximation SOBCM presents the smallest computational cost, requiring 44 additions only. Although $\hat{\mathbf{C}}_{16,1}$ needs four extra additions, it outperforms SOBCM, as shown in Tables 4 and 5. Among the transforms that require 52 additions, $\hat{\mathbf{C}}_{16,4}$ achieves the smallest total error energy, and $\hat{\mathbf{C}}_{16,5}$ is the best-performing in terms of MSE, coding gain, and transform efficiency measures. Approximation $\hat{\mathbf{C}}_{16,9}$ performs better than competing approaches that require 56 additions under all considered metrics. Among the transforms that require 60 additions, JAM₁₆ DCT approximation is the best-performing in all evaluated metrics, except transform efficiency, which is maximized for $\hat{\mathbf{C}}_{16,13}$. The approximation ABM₁₆ is the best approximation among the considered 64-addition transforms under all discussed metrics.

4.2 Novel 32-point DCT approximations

Analogously to the 16-point case described in the previous section, we submitted the discussed 8-point DCT approximation formalism (Equation (3)) to two instantiations of the JAM method. The resulting 32×32 DCT approximation

Table 6: Results for the novel 32-point DCT approximations.

j	$\epsilon(\cdot)$	MSE(\cdot)	$C_g^*(\cdot)$	$\eta(\cdot)$	$\mathcal{A}(\cdot)$	$\mathcal{S}(\cdot)$
1	68.13	0.13	8.23	56.18	128	0
2	65.78	0.13	8.23	56.05	136	0
3	60.57	0.13	8.23	56.43	136	4
4	59.47	0.13	8.23	56.78	136	4
5	63.93	0.12	8.44	56.72	136	8
6	60.69	0.12	8.25	56.47	144	0
7	57.12	0.12	8.23	56.65	144	4
8	58.22	0.12	8.23	56.31	144	4
9	55.27	0.12	8.44	57.33	144	12
10	56.37	0.12	8.44	56.98	144	12
11	52.23	0.12	8.27	56.03	152	0
12	56.49	0.12	8.46	57.01	152	8
13	52.93	0.12	8.44	57.57	152	8
14	48.04	0.12	8.48	56.57	160	8
15	48.73	0.12	8.65	58.14	160	16

Table 7: Results for competing 32-point DCT approximations.

Transform	$\epsilon(\cdot)$	MSE(\cdot)	$C_g^*(\cdot)$	$\eta(\cdot)$	$\mathcal{A}(\cdot)$	$\mathcal{S}(\cdot)$
JAM ₃₂ [45]	48.10	0.11	8.50	56.97	152	0
BAS ₃₂ -2013 [17]	192.18	0.76	8.27	55.91	160	0
BAS ₃₂ -2010 [34]	117.07	0.24	8.50	58.50	160	16
ABM ₃₂ [35]	46.27	0.11	8.95	61.03	160	24

matrices have the following characterization:

$$\mathbf{T}_{32}(\mathbf{a}) = \begin{bmatrix} \mathbf{T}_{16}(\mathbf{a}) & \mathbf{0}_{16} \\ \mathbf{0}_{16} & \mathbf{T}_{16}(\mathbf{a}) \end{bmatrix} \cdot \begin{bmatrix} \mathbf{I}_{16} & \bar{\mathbf{I}}_{16} \\ \mathbf{I}_{16} & -\bar{\mathbf{I}}_{16} \end{bmatrix}$$

where $\mathbf{0}_{16}$ is 16×16 a matrix of zeros; \mathbf{I}_{16} and $\bar{\mathbf{I}}_{16}$ are the identity and counter-identity matrices of order 16.

The similarity to the DCT and coding efficiency measurements for all the optimal 8-point DCT approximations scaled to 32×32 are shown in Table 6, and the 32-point DCT approximations are denoted by $\hat{\mathbf{C}}_{32,j}$, $j = 1, 2, \dots, 15$. To the best of our knowledge, the fifteen 32-point transforms listed in Table 6 are new contributions to literature. For comparison purposes, Table 7 lists the performance of 32-point approximations found in literature [17, 34, 35, 45].

One may notice that the proposed 32-point DCT approximations demand 15% fewer additions than any previously reported transform. Among the DCT approximations that require 136 additions, $\hat{\mathbf{C}}_{32,4}$ is the best-performing in terms of total error energy and transform efficiency; whereas $\hat{\mathbf{C}}_{32,5}$ performed well in terms of MSE and coding gain. Similar behavior can be seen for transforms requiring 144 additions. Regarding transforms demanding 152 additions, $\hat{\mathbf{C}}_{32,13}$ outperforms the 32-point approximate DCT in [45] in terms of transform efficiency. Finally, ABM₃₂ is the best-performing among approximations requiring 160 additions.

5 Image compression experiments

In order to further assess the performance of the best-performing transforms we adopted the JPEG-like image compression experiment detailed in [20, 24, 31–34]. We present the average results for 45 512×512 grayscale images taken from the public image database available in [57]. In this experiment, the input images are firstly subdivided into blocks of size 8×8 , 16×16 , and 32×32 , depending on the considered transform size. Then, each block is forward transformed through (1), resulting in a blockwise transformed image. The transformed blocks are submitted

to a simplified quantization step where the first r coefficients, according to the zig-zag sequence [46], are retained and the remainder are set to zero. Although the zig-zag sequence could easily be modified to better suit the considered transforms, we maintained the standard zig-zag to facilitate fair comparison with other methods in literature. Here, r ranges from 25% to 99% the number of coefficients per block. Finally, the blockwise inverse transform in (2) is applied. In Equations (1) and (2) we replaced the transform matrix \mathbf{C}_N by each optimal DCT approximation $\hat{\mathbf{C}}_{N,j}$, $j = 1, 2, \dots, 15$ and $N = 8, 16, 32$.

From the compressed images, we measure the peak signal-to-noise ratio (PSNR) [58] and the structural similarity index (SSIM) [59]. The former is a traditional and widely used metric for image quality assessment [58]. The latter is a complementary figure of merit for evaluating image quality that considers luminance, contrast, and structure of the image to quantify degradation, approaching to a subjective assessment [15]. Besides presenting the average PSNR and SSIM curves, for better visualization, we show their absolute percentage error (APE) [60]. The presented APE results consider the DCT-based measurements as baseline.

For the 8-point transforms, Figures 3(a), 3(b), 3(c) and 3(d) show that the ABM approximation performs the best. Considering transforms that require 20 addition, $\hat{\mathbf{C}}_{8,9}$ offers the best results and FW_6 performs unfavorably. These results corroborate the coding gain measurements presented in Tables 2 and 3. Additionally, Figures 3(e) and 3(f) show the gain in terms of PSNR and SSIM per addition operation. The approximation $\hat{\mathbf{C}}_{8,1}$ offered the highest PSNR and SSIM gain per addition. A median behavior is achieved by $\hat{\mathbf{C}}_{8,9}$ in terms of PSNR, SSIM, and the gains by addition. The only transforms requiring 20 additions are found in [23]. Thus the approximation $\hat{\mathbf{C}}_{8,9}$ is the best one at 20 additions.

Considering 16-point DCT approximations, according to Figures 4(a), 4(b), 4(c) and 4(d), the approximation ABM_{16} was the best-performing. Approximation $\hat{\mathbf{C}}_{16,1}$ has the highest PSNR and SSIM gain per additive cost unit, as shown in Figures 4(e) and 4(f). As for the case of 8-point transforms, $\hat{\mathbf{C}}_{16,9}$ has a median behavior for all the considered metrics in this image compression experiment. In this case, to the best of our knowledge, there are not 48-, 52- or 56-addition methods for a direct comparison. Therefore the proposed transforms, $\hat{\mathbf{C}}_{16,1}$, $\hat{\mathbf{C}}_{16,4}$, $\hat{\mathbf{C}}_{16,5}$, and $\hat{\mathbf{C}}_{16,9}$ stand alone as best in their classes.

Transforms of sizes 16×16 and 32×32 behave very similarly, as shown in Figures 4 and 5 for the 32-point case. Approximations $\hat{\mathbf{C}}_{32,1}$, $\hat{\mathbf{C}}_{32,4}$, $\hat{\mathbf{C}}_{32,5}$, $\hat{\mathbf{C}}_{32,6}$, and $\hat{\mathbf{C}}_{32,9}$ have lower arithmetic complexity than any already known 32-point DCT approximations in literature. Transform $\hat{\mathbf{C}}_{32,1}$ has the smaller computational complexity. For a range of r values the transform $\hat{\mathbf{C}}_{32,13}$ is outperformed by JAM_{32} . As far as we know, a 32-point transform requiring less than 152 additions is absent in literature. As a consequence, transforms $\hat{\mathbf{C}}_{32,1}$, $\hat{\mathbf{C}}_{32,4}$, $\hat{\mathbf{C}}_{32,5}$, $\hat{\mathbf{C}}_{32,6}$, and $\hat{\mathbf{C}}_{32,9}$ are identified as best performing tools. The main behavior of the optimal BAS-based 8-point transforms is preserved when scaling them to transforms of size 16×16 and 32×32 using the JAM algorithm.

6 Video coding experiments

In this section, we show the applicability of the best-performing multiparametric DCT approximations— $\hat{\mathbf{C}}_{8,1}$, $\hat{\mathbf{C}}_{8,5}$, and $\hat{\mathbf{C}}_{8,9}$ and their 16- and 32-point scaled versions—in the context of video coding. We embedded the selected transforms into the public available HEVC reference software provided in [61], then we assessed the performance of the resulting systems. The HEVC improves its predecessors [44] and aims at providing high video compression rates [9]. Unlike H.264 and older video coding standards, the HEVC standard employs not only an 8-point DCT but also transforms of length 4, 16, and 32 for better handling smooth and textured image regions of various sizes [9].

In our experiments, we replace the original 8-, 16-, and 32-point HEVC transforms by the three selected DCT approximations and their scaled versions, one at a time. We shall call $\hat{\mathbf{C}}_1$, $\hat{\mathbf{C}}_5$, and $\hat{\mathbf{C}}_9$ each set of transforms based on $\hat{\mathbf{C}}_{8,1}$, $\hat{\mathbf{C}}_{8,5}$, and $\hat{\mathbf{C}}_{8,9}$, respectively. The original 4-point HEVC transform was kept unchanged because it is already a low-complexity transformation. We encoded the first 100 frames of one video sequence of each A to F class following the recommendations in the Common Test Conditions (CTC) documentation [62]. Namely we used the following 8-bit

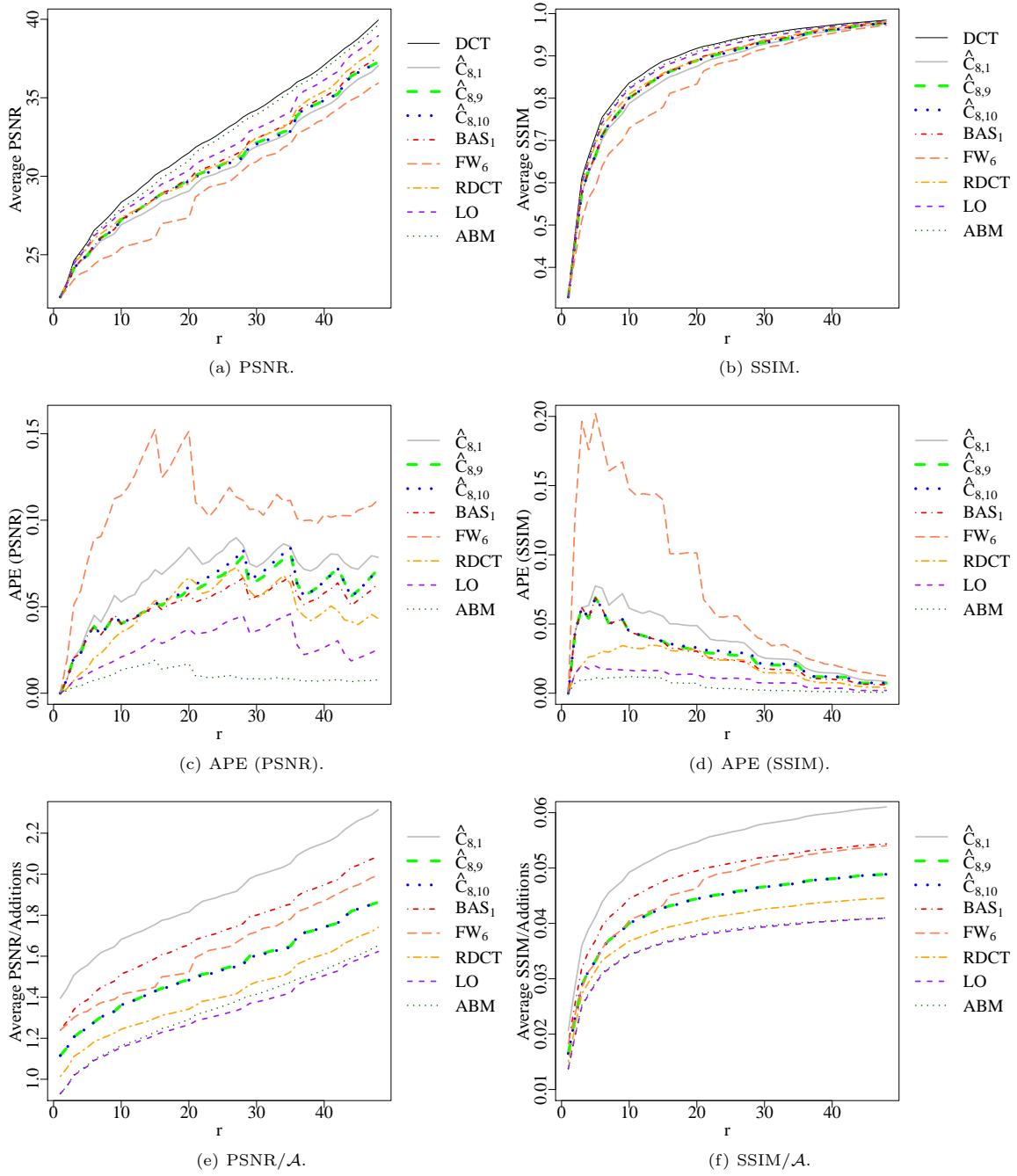


Figure 3: Image compression results for novel and competing 8-point DCT approximations.

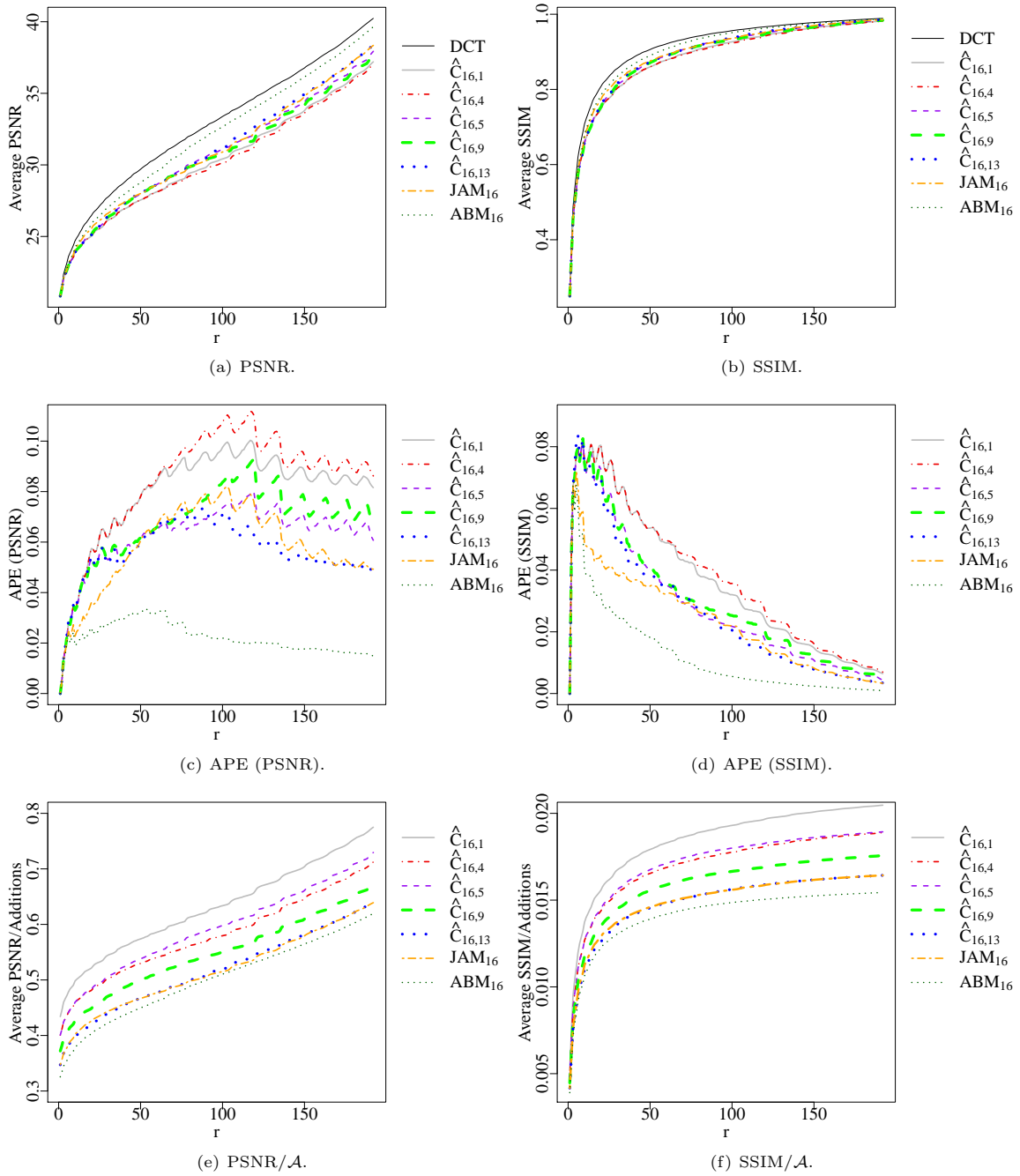


Figure 4: Image compression results for novel and competing 16-point DCT approximations.

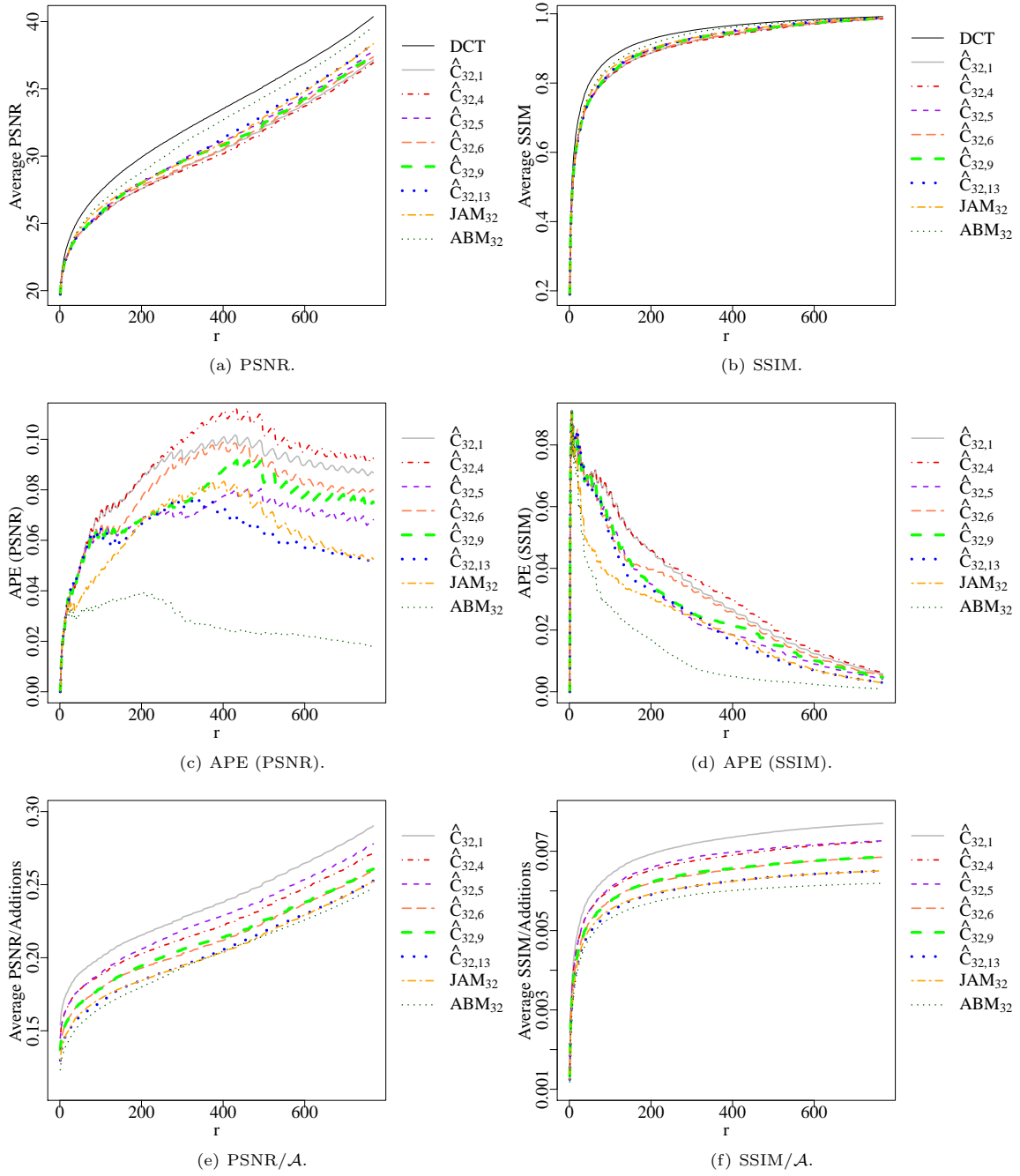


Figure 5: Image compression results for novel and competing 32-point DCT approximations.

Table 8: Average Bjøntegaard’s metrics for the modified versions of the HEVC reference software.

Config.	Video sequence	BD-PSNR (dB)			BD-Rate (%)		
		\hat{C}_1	\hat{C}_5	\hat{C}_9	\hat{C}_1	\hat{C}_5	\hat{C}_9
AI	“PeopleOnStreet”	-0.495	-0.465	-0.465	9.870	9.251	9.246
	“BasketballDrive”	-0.267	-0.250	-0.253	10.474	9.771	9.870
	“RaceHorses”	-0.622	-0.609	-0.596	8.135	7.970	7.795
	“BlowingBubbles”	-0.219	-0.203	-0.203	3.880	3.601	3.600
	“KristenAndSara”	-0.415	-0.389	-0.392	8.628	8.100	8.143
	“BasketballDrillText”	-0.172	-0.162	-0.162	3.358	3.160	3.168
RA	“PeopleOnStreet”	-0.264	-0.244	-0.245	6.484	5.985	6.009
	“BasketballDrive”	-0.214	-0.199	-0.203	10.060	9.330	9.547
	“RaceHorses”	-0.816	-0.780	-0.746	13.857	13.264	12.762
	“BlowingBubbles”	-0.158	-0.144	-0.148	4.296	3.891	4.014
	“BasketballDrillText”	-0.223	-0.207	-0.207	5.573	5.151	5.153
LDB	“BasketballDrive”	-0.201	-0.187	-0.190	8.899	8.242	8.395
	“RaceHorses”	-0.805	-0.771	-0.739	12.674	12.138	11.678
	“BlowingBubbles”	-0.160	-0.151	-0.153	4.442	4.193	4.243
	“KristenAndSara”	-0.200	-0.180	-0.187	7.081	6.319	6.525
LDP	“BasketballDrillText”	-0.267	-0.243	-0.251	7.029	6.382	6.580
	“BasketballDrive”	-0.203	-0.187	-0.192	8.945	8.173	8.459
	“RaceHorses”	-0.775	-0.744	-0.715	12.094	11.607	11.203
	“BlowingBubbles”	-0.150	-0.138	-0.139	4.267	3.906	3.964
	“KristenAndSara”	-0.179	-0.163	-0.168	6.668	6.016	6.244
	“BasketballDrillText”	-0.246	-0.227	-0.234	6.565	6.057	6.222

videos: “PeopleOnStreet” (2560×1600 at 30 fps), “BasketballDrive” (1920×1080 at 50 fps), “RaceHorses” (832×480 at 30 fps), “BlowingBubbles” (416×240 at 50 fps), “KristenAndSara” (1280×720 at 60 fps), and “BasketballDrillText” (832×480 at 50 fps). All the encoding parameters were also set according to CTC documentation for the Main profile and All-Intra (AI), Random Access (RA), Low Delay B (LD-B), and Low Delay P (LD-P) configurations.

For assessing image quality, we use the per color channel MSE (MSE-Y, MSE-U, and MSE-V) and PSNR (PSNR-Y, PSNR-U, and PSNR-V), for each video frame [43]. Such measurements are collected by the reference software. From those values, we also calculate the Bjøntegaard’s delta PSNR (BD-PSNR) and delta rate (BD-Rate) [63, 64] for all discussed transform sets and configurations. The BD-PSNR and BD-Rate measurements for each video sequence are summarized in Table 8.

The approximation \hat{C}_5 performed slightly better performance than \hat{C}_9 in most cases. Replacing the original HEVC transforms by either \hat{C}_5 or \hat{C}_9 results in a loss of no more than 0.60 dB at AI configuration. Finally, note that both transforms \hat{C}_5 and \hat{C}_9 have consistently better results than \hat{C}_1 in terms of BD-PSNR and BD-Rate. These findings reinforce the results from the still image compression experiments in the previous section.

For qualitative assessment, Figure 6 illustrates the tenth frame of the “BlowingBubbles” video sequence using the original HEVC configurations and the modified versions of the reference software after embedding the discussed 8-, 16-, and 32-point DCT approximations. Such results consider the main AI configuration mode and the quantization parameter (QP) set to 32.

The video frame in Figure 6 show that any existing visual degradation are essentially imperceptible; and therefore the switching from the original HEVC transforms to the proposed multiparametric low-complexity DCT approximations does not result in significant losses. Table 9 summarizes the quantitative measurements related to the video frame shown in Figure 6. One may note that for the given video frame, our modified HEVC reference software may lead to better results than the original one in terms of MSE and PSNR depending on the color channel.

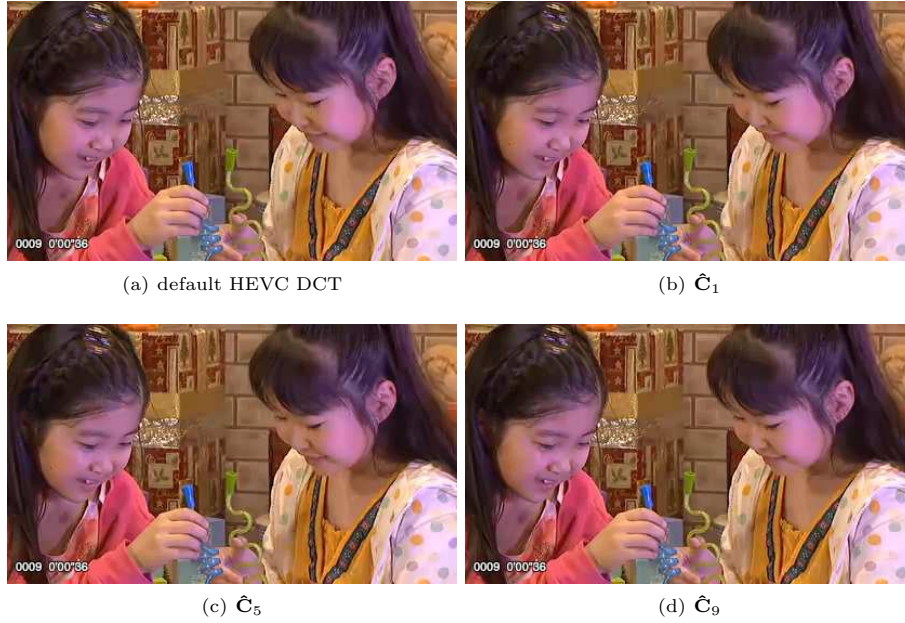


Figure 6: Compressed frame of “BlowingBubbles” using AI coding configuration with $QP = 32$. Core transforms are the default HEVC DCT, and the low-complexity DCT approximations.

Table 9: MSE and PSNR measurements for compressed frame of “BlowingBubbles” using AI coding configuration with $QP = 32$.

	HEVC DCT	\hat{C}_1	\hat{C}_5	\hat{C}_9
MSE-Y	30.957	31.229	31.065	30.763
MSE-U	13.793	13.769	13.689	14.092
MSE-V	9.934	10.187	10.006	9.731
PSNR-Y (dB)	33.223	33.175	33.201	33.250
PSNR-U (dB)	36.734	36.742	36.767	36.641
PSNR-V (dB)	38.159	38.050	38.128	38.249

7 Conclusion

In this work, we proposed a novel class of low-complexity transforms based on the mathematical frameworks introduced by [17, 24, 31, 33, 34]. We have presented a parametrized fast algorithm linked to the introduced 8-point DCT approximations. Based on a multicriteria optimization scheme, we could jointly optimize the coding efficiency metrics and the distance between the candidate transforms to the exact DCT in order to identify the best-performing 8-point approximations. As a result, we obtained fifteen optimal DCT approximations, which were submitted to the JAM scaling method for obtaining novel 16- and 32-point transforms.

The obtained 8-point and scaled transforms were assessed in terms of computational complexity, coding efficiency, and similarity to the DCT. Furthermore, we submitted the introduced 8-, 16- and 32-point transforms to both image and videos coding experiments along with extensive comparisons with competing low-complexity DCT approximations. Results show that the proposed DCT approximations can outperform several peering methods in terms of image and video coding quality metrics. We emphasize that the very low complexity of the proposed transforms can be fundamental for efficient hardware implementation in scenarios of limited resources (energy autonomy or processing power) and real-time encoding, as illustrated in the context of wireless visual sensor networks.

Further research in this area can be pursued in terms of deriving low-complexity methods for non-trigonometric transforms, such as discrete wavelet transforms. However, discrete wavelets constitute a fundamentally different approach when compared to usual trigonometric transforms, such as the DCT. Therefore, new tools and comparison procedures are expected to be derived.

Acknowledgments

We gratefully acknowledge partial financial support from Fundação de Amparo a Ciência e Tecnologia do Estado de Pernambuco (FACEPE), Conselho Nacional de Desenvolvimento Científico and Tecnológico (CNPq), and Coordenação de Aperfeiçoamento de Pessoal de Nível Superior (CAPES), Brazil.

References

- [1] N. Ahmed, T. Natarajan, and K. Rao, "Discrete cosine transform," *IEEE Transactions on Computers*, vol. 23, no. 1, pp. 90–93, 1974. 1, 2
- [2] N. Ahmed and K. R. Rao, *Orthogonal Transforms for Digital Signal Processing*. Berlin: Springer-Verlag, 1975. 1, 2
- [3] A. V. Oppenheim and R. W. Schaffer, *Discrete-Time Signal Processing*, 3rd ed. Upper Saddle River, NJ, USA: Prentice Hall Press, 2009. 1
- [4] M. Effros, H. Feng, and K. Zeger, "Suboptimality of the Karhunen-Loève transform for transform coding," *IEEE Transactions on Information Theory*, vol. 50, no. 8, pp. 1605–1619, Aug. 2004. 1
- [5] R. J. Clark, "Relation between Karhunen-Loève and cosine transform," in *IEE Proceedings-F, Communications, Radar and Signal Processing*, vol. 128, no. 6, 1981, pp. 359–360. 1
- [6] R. C. Gonzalez and R. E. Woods, *Digital image processing*. Upper Saddle River, N.J.: Prentice Hall, 2008. 1
- [7] JPEG, "Joint photographic experts group," 2012. [Online]. Available: <http://www.jpeg.org> 1
- [8] T. Wiegand, G. J. Sullivan, G. Bjøntegaard, and A. Luthra, "Overview of the H.264/AVC video coding standard," *IEEE Transactions on Circuits and Systems for Video Technology*, vol. 13, no. 7, pp. 560–576, Jul. 2003. 1
- [9] M. T. Pourazad, C. Doutre, M. Azimi, and P. Nasiopoulos, "HEVC: The new gold standard for video compression: How does HEVC compare with H.264/AVC?" *IEEE Consumer Electronics Magazine*, vol. 1, no. 3, pp. 36–46, Jul. 2012. 1, 2, 9, 13
- [10] W. H. Chen, C. Smith, and S. Fralick, "A fast computational algorithm for the discrete cosine transform," *IEEE Transactions on Communications*, vol. 25, no. 9, pp. 1004–1009, 1977. 1
- [11] B. G. Lee, "A new algorithm for computing the discrete cosine transform," *IEEE Transactions on Acoustics, Speech and Signal Processing*, vol. ASSP-32, pp. 1243–1245, Dec. 1984. 1
- [12] C. Loeffler, A. Ligtenberg, and G. Moschytz, "Practical fast 1D DCT algorithms with 11 multiplications," in *Proceedings of the International Conference on Acoustics, Speech, and Signal Processing*, 1989, pp. 988–991. 1

- [13] F. Feig and S. Winograd, "Fast algorithms for the discrete cosine transform," *IEEE Transactions on Signal Processing*, vol. 40, no. 9, pp. 2174–2193, 1992. 1
- [14] V. Britanak, P. Yip, and K. R. Rao, *Discrete Cosine and Sine Transforms*. Academic Press, 2007. 1, 3, 6, 7
- [15] Z. Wang and A. C. Bovik, "Reduced- and no-reference image quality assessment," *IEEE Signal Processing Magazine*, vol. 28, no. 6, pp. 29–40, 2011. 1, 13
- [16] S. Saponara, "Real-time and low-power processing of 3D direct/inverse discrete cosine transform for low-complexity video codec," *Journal of Real-Time Image Processing*, vol. 7, no. 1, pp. 43–53, Mar. 2012. 1
- [17] S. Bouguezel, M. O. Ahmad, and M. N. S. Swamy, "Binary discrete cosine and Hartley transforms," *IEEE Transactions on Circuits and Systems I: Regular Papers*, vol. 60, no. 4, pp. 989–1002, 2013. 1, 2, 3, 9, 11, 12, 19
- [18] N. Kouadria, N. Doghmane, D. Messadeg, and S. Harize, "Low complexity DCT for image compression in wireless visual sensor networks," *Electronics Letters*, vol. 49, no. 24, pp. 1531–1532, Nov. 2013. 1
- [19] N. Kouadria, K. Mechouek, D. Messadeg, and N. Doghmane, "Pruned discrete Tchebichef transform for image coding in wireless multimedia sensor networks," *AEU - International Journal of Electronics and Communications*, vol. 74, pp. 123–127, 2017. 1
- [20] T. I. Haweel, "A new square wave transform based on the DCT," *Signal Processing*, vol. 82, pp. 2309–2319, 2001. 1, 3, 12
- [21] F. M. Bayer and R. J. Cintra, "DCT-like transform for image compression requires 14 additions only," *Electronics Letters*, vol. 48, no. 15, pp. 919–921, 2012. 1, 3, 6, 7
- [22] R. J. Cintra and F. M. Bayer, "A DCT approximation for image compression," *IEEE Signal Processing Letters*, vol. 18, no. 10, pp. 579–582, 2011. 1, 3, 6, 7, 9
- [23] C. J. Tablada, F. M. Bayer, and R. J. Cintra, "A class of DCT approximations based on the Feig-Winograd algorithm," *Signal Processing (Print)*, vol. 11, pp. 1–20, 2015. 1, 3, 7, 9, 13
- [24] S. Bouguezel, M. O. Ahmad, and M. N. S. Swamy, "A low-complexity parametric transform for image compression," in *Proceedings of the 2011 IEEE International Symposium on Circuits and Systems*, 2011, pp. 2145–2148. 1, 2, 3, 7, 9, 12, 19
- [25] U. S. Potluri, A. Madanayake, R. J. Cintra, F. M. Bayer, and N. Rajapaksha, "Multiplier-free DCT approximations for RF multi-beam digital aperture-array space imaging and directional sensing," *Measurement Science and Technology*, vol. 23, no. 11, p. 114003, 2012. 1, 6
- [26] U. S. Potluri, A. Madanayake, R. J. Cintra, F. M. Bayer, S. Kulasekera, and A. Edirisuriya, "Improved 8-point approximate DCT for image and video compression requiring only 14 additions," *IEEE Transactions on Circuits and Systems I*, vol. 61, no. 6, pp. 1727–1740, 2013. 1
- [27] F. M. Bayer and R. J. Cintra, "Image compression via a fast DCT approximation," *IEEE Latin America Transactions*, vol. 8, no. 6, pp. 708–713, Dec. 2010. 1
- [28] F. M. Bayer, R. J. Cintra, A. Edirisuriya, and A. Madanayake, "A digital hardware fast algorithm and FPGA-based prototype for a novel 16-point approximate DCT for image compression applications," *Measurement Science and Technology*, vol. 23, no. 8, pp. 114010–114019, 2012. 1, 7, 11
- [29] F. M. Bayer, R. J. Cintra, A. Madanayake, and U. S. Potluri, "Multiplierless approximate 4-point DCT VLSI architectures for transform block coding," *Electronics Letters*, vol. 49, no. 24, pp. 1532–1534, Nov. 2013. 1
- [30] R. J. Cintra, F. M. Bayer, and C. J. Tablada, "Low-complexity 8-point DCT approximations based on integer functions," *Signal Processing*, vol. 99, pp. 201–214, 2014. 1
- [31] S. Bouguezel, M. O. Ahmad, and M. N. S. Swamy, "Low-complexity 8×8 transform for image compression," *Electronics Letters*, vol. 44, no. 21, pp. 1249–1250, Sep. 2008. 1, 2, 3, 7, 8, 9, 12, 19
- [32] —, "A multiplication-free transform for image compression," in *2nd International Conference on Signals, Circuits and Systems*, Nov. 2008, pp. 1–4. 1, 2, 12
- [33] —, "A fast 8×8 transform for image compression," in *2009 International Conference on Microelectronics (ICM)*, Dec. 2009, pp. 74–77. 1, 2, 3, 7, 8, 9, 12, 19
- [34] —, "A novel transform for image compression," in *53rd IEEE International Midwest Symposium on Circuits and Systems (MWSCAS)*, Aug. 2010, pp. 509–512. 1, 2, 3, 7, 8, 9, 11, 12, 19
- [35] R. S. Oliveira, R. J. Cintra, F. M. Bayer, T. L. T. da Silveira, A. Madanayake, and A. Leite, "Low-complexity 8-point DCT approximation based on angle similarity for image and video coding," *Multidimensional Systems and Signal Processing*, vol. 30, no. 3, pp. 1363–1394, Jul. 2019. 1, 3, 9, 11, 12
- [36] V. A. Coutinho, R. J. Cintra, and F. M. Bayer, "Low-complexity multidimensional DCT approximations for high-order tensor data decorrelation," *IEEE Transactions on Image Processing*, vol. 26, no. 5, pp. 2296–2310, 2017. 1
- [37] R. Ezhilarasi, K. Venkatalakshmi, and B. Khanth, "Enhanced approximate discrete cosine transforms for image compression and multimedia applications," *Multimedia Tools and Applications*, vol. (Online First), pp. 1–14, 2018. 1
- [38] H. A. F. Almurib, T. N. Kumar, and F. Lombardi, "Approximate DCT image compression using inexact computing," *IEEE Transactions on Computers*, vol. 67, no. 2, pp. 149–159, 2018. 1
- [39] J. Zhang, W. Shi, L. Zhou, R. Gong, L. Wang, and H. Zhou, "A low-power and high-PSNR unified DCT/IDCT architecture based on EARC and enhanced scale factor approximation," *IEEE Access*, vol. 7, pp. 165 684–165 691, 2019. 1

- [40] J. Huang, T. Nandha Kumar, H. A. F. Almurib, and F. Lombardi, "A deterministic low-complexity approximate (multiplierless) technique for DCT computation," *IEEE Transactions on Circuits and Systems I: Regular Papers*, vol. 66, no. 8, pp. 3001–3014, 2019. 1
- [41] N. Zidani, N. Kouadria, N. Doghmane, and S. Harize, "Low complexity pruned DCT approximation for image compression in wireless multimedia sensor networks," in *2019 5th International Conference on Frontiers of Signal Processing (ICFSP)*, Sep. 2019, pp. 26–30. 1
- [42] N. Brahimi, T. Bouden, T. Brahimi, and L. Boubchir, "A novel and efficient 8-point DCT approximation for image compression," *Multimedia Tools and Applications*, vol. (Online First), pp. 1–17, 2020. 1, 3, 7, 8
- [43] J.-R. Ohm, G. J. Sullivan, H. Schwarz, T. K. Tan, and T. Wiegand, "Comparison of the coding efficiency of video coding standards - including high efficiency video coding (HEVC)," *IEEE Transactions on Circuits and Systems for Video Technology*, vol. 22, no. 12, pp. 1669–1684, Dec. 2012. 1, 17
- [44] G. J. Sullivan, J. R. Ohm, W. J. Han, and T. Wiegand, "Overview of the high efficiency video coding (HEVC) standard," *IEEE Transactions on Circuits and Systems for Video Technology*, vol. 22, no. 12, pp. 1649–1668, 2012. 2, 13
- [45] M. Jridi, A. Alfalou, and P. K. Meher, "A generalized algorithm and reconfigurable architecture for efficient and scalable orthogonal approximation of DCT," *IEEE Transactions on Circuits and Systems I: Regular Papers*, vol. 62, no. 2, pp. 449–457, 2015. 2, 9, 11, 12
- [46] G. K. Wallace, "The JPEG still picture compression standard," *IEEE Transactions on Consumer Electronics*, vol. 30, no. 1, pp. xviii–xxxiv, 1992. 2, 13
- [47] K. Lengwehasatit and A. Ortega, "Scalable variable complexity approximate forward DCT," *IEEE Transactions on Circuits and Systems for Video Technology*, vol. 14, no. 11, pp. 1236–1248, Nov. 2004. 6, 7, 9
- [48] R. J. Cintra, "An integer approximation method for discrete sinusoidal transforms," *Circuits, Systems, and Signal Processing*, vol. 30, pp. 1481–1501, 2011. 7
- [49] N. J. Higham, "Computing real square roots of a real matrix," *Linear Algebra and its Applications*, vol. 88–89, pp. 405–430, 1987. 7
- [50] N. S. Jayant and P. Noll, *Digital Coding of Waveforms, Principles and Applications to Speech and Video*. Englewood Cliffs NJ, USA: Prentice-Hall, 1984, p. 688. 7
- [51] R. Core Team, *R: A Language and Environment for Statistical Computing*, R Foundation for Statistical Computing, Vienna, Austria, 2016. [Online]. Available: <https://www.R-project.org/> 7
- [52] R. S. Oliveira, R. J. Cintra, F. M. Bayer, and C. J. Tablada, "Uma aproximação ortogonal para a DCT," in *XXXI Simpósio Brasileiro de Telecomunicações*, 2013. 7, 8, 9
- [53] N. Brahimi and S. Bouguezel, "An efficient fast integer DCT transform for images compression with 16 additions only," in *International Workshop on Systems, Signal Processing and their Applications*, 2011, 71–74. 7
- [54] K. Miettinen, *Nonlinear Multiobjective Optimization*, ser. International Series in Operations Research and Management Science. Kluwer Academic Publishers, Dordrecht, 1999, vol. 12. 9
- [55] T. L. T. da Silveira, F. M. Bayer, R. J. Cintra, S. Kulasekera, A. Madanayake, and A. J. Kozakevicius, "An orthogonal 16-point approximate DCT for image and video compression," *Multidimensional Systems and Signal Processing*, vol. 27, no. 1, pp. 87–104, 2016. 9, 11
- [56] T. L. T. da Silveira, R. S. Oliveira, F. M. Bayer, R. J. Cintra, and A. Madanayake, "Multiplierless 16-point DCT approximation for low-complexity image and video coding," *Signal, Image and Video Processing*, vol. 11, no. 2, pp. 227–233, 2017. 9, 11
- [57] (2011) USC-SIPI: The USC-SIPI Image Database. University of Southern California, Signal and Image Processing Institute. <http://sipi.usc.edu/database/>. University of Southern California, Signal and Image Processing Institute. [Online]. Available: <http://sipi.usc.edu/database/> 12
- [58] Q. H. Thu and M. Ghanbari, "Scope of validity of PSNR in image/video quality assessment." *Electronics Letters*, vol. 44, no. 13, pp. 800–801, 2008. 13
- [59] Z. Wang, A. C. Bovik, H. R. Sheikh, and E. P. Simoncelli, "Image quality assessment: from error visibility to structural similarity," *IEEE Transactions on Image Processing*, vol. 13, no. 4, pp. 600–612, 2004. 13
- [60] N. J. Higham, *Functions of matrices: theory and computation*. SIAM, 2008, vol. 104. 13
- [61] Joint Collaborative Team on Video Coding (JCT-VC), "HEVC reference software documentation," 2013, Fraunhofer Heinrich Hertz Institute. [Online]. Available: <https://hevc.hhi.fraunhofer.de/> 13
- [62] F. Bossen, "Common test conditions and software reference configurations," San Jose, CA, USA, Feb. 2013, document JCT-VC L1100. 13
- [63] G. Bjøntegaard, "Calculation of average PSNR differences between RD-curves," in *13th VCEG Meeting*, Austin, TX, USA, Apr. 2001, document VCEG-M33. 17
- [64] P. Hanhart and T. Ebrahimi, "Calculation of average coding efficiency based on subjective quality scores," *Journal of Visual Communication and Image Representation*, vol. 25, no. 3, pp. 555 – 564, 2014. 17